Journal of Applied Physics

RESEARCH ARTICLE | MAY 16 2023

Radio frequency cantilever-free scanning probe microscopy

Gwangmook Kim; YoungJun Cho; Min-Kyun Cho; ... et. al

Journal of Applied Physics 133, 194504 (2023)
https://doi.org/10.1063/5.0152880

AIP Publishing

Journal of Applied Physics METHOD scitation.org/journal/jap

Radio frequency cantilever-free scanning probe microscopy

Cite as: J. Appl. Phys. 133, 194504 (2023); doi: 10.1063/5.0152880
Submitted: 2 April 2023 · Accepted: 4 May 2023 ·
Published Online: 16 May 2023

Gwangmook Kim,[1] YoungJun Cho,[1,2,3] Min-Kyun Cho,[4] Dohun Kim,[4] and Wooyoung Shim[1,2,3,a)]

AFFILIATIONS

[1]Department of Materials Science and Engineering, Yonsei University, Seoul 03722, Republic of Korea
[2]Center for Multi-Dimensional Materials, Yonsei University, Seoul 03722, Republic of Korea
[3]Center for NanoMedicine, Institute for Basic Science (IBS), Seoul 03722, Republic of Korea
[4]Department of Physics and Astronomy and Institute of Applied Physics, Seoul National University, Seoul 08826, Republic of Korea

[a)]**Author to whom correspondence should be addressed:** wshim@yonsei.ac.kr

ABSTRACT

Cantilever-free scanning probe microscopy has enormous potential for high-throughput topography imaging using parallel probe arrays. However, the current imaging mechanism of the cantilever-free tip architecture hardly considers the efficiency of the detection method regarding precision and bandwidth, which could be a bottleneck to expanding the application of this measurement system. In this communication, we present a contact resistance-based cantilever-free imaging system using radio frequency (RF) reflectometry. RF reflectometry measurements provide sensitive detection of the contact resistance with a wide bandwidth, enabling sub-micrometer-scale topography imaging. We demonstrated our imaging system using a carbon black-polydimethylsiloxane composite tip with a custom-built RF reflectometry setup. The proof-of-concept system achieved a resolution of 230 nm and a bandwidth of the detection system of approximately 8.5 MHz, validating the feasibility of the imaging technique for potential high-throughput cantilever-free scanning probe microscopy.

I. INTRODUCTION

Scanning probe microscopy (SPM) is a routine high-resolution inspection tool to resolve various specimens such as two-dimensional (2D) materials,[1] surface structures,[2] and biomolecules.[3] However, the slow imaging speed and narrow field of view of SPM hinder an expansion of its applications beyond scientific research. Achieving high throughput has been an important development goal of SPM. SPM methodologies, e.g., scanning tunneling microscopy (STM)[4] and atomic force microscopy (AFM),[5] are inherently unfavorable for large-area measurements because of the serial nature of mechanical scans imposing low bandwidth. Effort has been devoted to addressing this limitation by means of a high bandwidth system[6–8] and parallel measurement approach using multiple probe arrays.[9–13] However, these approaches have a limited field-of-view, and the probe array and detection system have a complex structure. Consequently, the application of typical SPM equipment still focuses on small features up to several tens of micrometers.

Recently, cantilever-free SPM systems harnessing massively parallel probe arrays have been developed for large-area measurements.[14,15] The cantilever-free tip architecture adopts an elastomeric buffer mechanism instead of a complex cantilever design, which enables fabricating multiple probe arrays using an uncomplicated process. While this architecture was initially proposed for high-throughput scanning probe lithography (SPL),[16–18] two pioneering works invented novel imaging mechanisms for cantilever-free tip architecture.[15] Cantilever-free SPM can measure a millimeter-scale field-of-view using a parallel probe array,[15] which validates the potential for high-throughput topography measurements.

Despite the achievement of cantilever-free SPM in facile fabrication, one of the remaining challenges is to design an efficient detection method to handle the overwhelming signals from a massively parallel probe array. Under the limited capacity of a detection system, increasing the number of probes causes a trade-off with the imaging rate and resolving power of an individual probe[15] and eventually negates the merits of parallel measurements. In this stage, the scalability of cantilever-free SPM is much smaller than that of

cantilever-free SPL owing to the limitation of the detection system.[16] Consequently, realizing massively parallel cantilever-free SPM demands an efficient imaging mechanism that allows both high precision and wide bandwidth of the detection system.

In this communication, we present a cantilever-free imaging mechanism adopting radio frequency (RF) reflectometry. RF reflectometry measurements detect the reflected signal at the resonance frequency of the LCR circuit. This detection method provides a precise electrical measurement using the sensitive change in reflectance near the impedance matching point. High temporal resolution with a bandwidth of a few MHz can be obtained by tuning the resonance frequency of the LCR circuit. Using a carbon black-polydimethylsiloxane (CB-PDMS) composite tip and the custom-built RF reflectometry setup, we demonstrated the proof-of-concept system to investigate the feasibility of RF cantilever-free imaging for nanoscale topography measurements with the potentially high-throughput detection system.

II. RESULTS AND DISCUSSION

The concept of the imaging mechanism is depicted in Fig. 1(a). The imaging mechanism is based on the contact resistance between the conductive elastomeric tip and surface. When the tip vertically scans the surface, the contact area of the elastomeric tip is determined by the height of the measured point, which can be quantified through contact resistance. During the imaging process, the tip repeats vertical scanning with a constant scanning distance [Fig. 1(b)]. Then, the contact resistance of each point is collected and reconstructed into the topography of the surface.

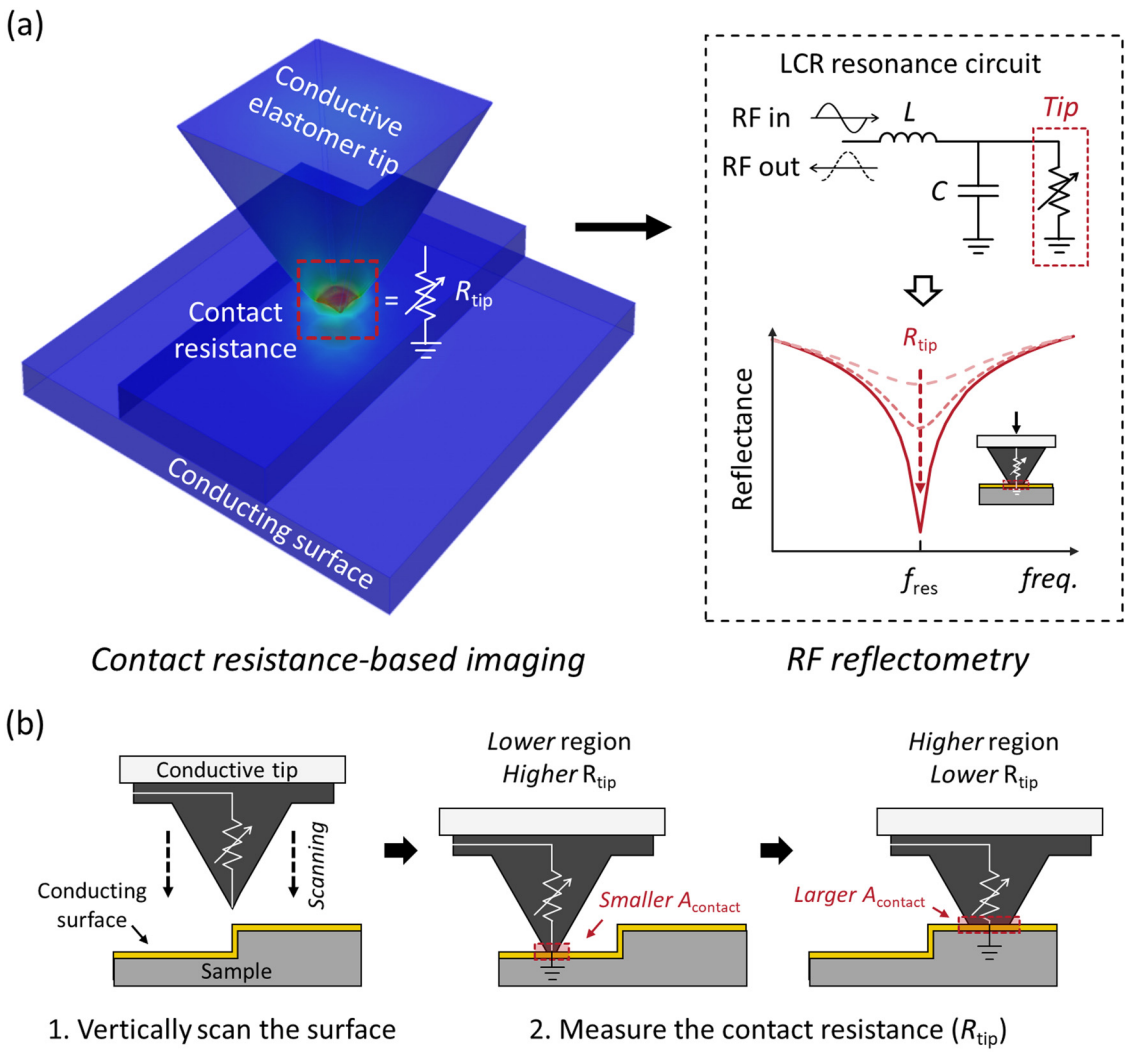

FIG. 1. Concept of RF cantilever-free scanning probe microscopy. (a) Schematic illustration of radio frequency (RF) cantilever-free scanning probe microscopy. (b) Principle of cantilever-free probe imaging based on contact resistance.

To detect the contact resistance, we exploited RF reflectometry measurement using the LCR impedance matching circuit. RF reflectometry is an electrical measurement technique that detects the impedance using the reflectance of a RF wave. RF reflectometry offers sensitive, fast electrical detection and has been used for the measurement of single electron transistors,[19] quantum dots,[20,21] and high-speed STM.[22] The wide bandwidth of RF reflectometry is potentially useful for constructing a high-capacity detection system of massively parallel cantilever-free SPM arrays.

The basic principle of RF reflectometry relies on the power transfer ratio, which is affected by the impedance of the RF source and the LCR circuit. When the RF wave is transferred to the LCR circuit, the reflectance can be expressed as follows:

$$\Gamma = (Z_L - Z_0)/(Z_L + Z_0), \tag{1}$$

where Γ, Z_L, and Z_0 are the reflection coefficient, load impedance of the LCR circuit, and output impedance of the RF source, respectively. The maximal power transfer occurs with no reflection ($\Gamma = 0$) at the impedance matching between the RF source and the LCR circuit ($Z_L = Z_0$). The change in reflectance near the impedance matching point provides a sensitive measurement of the contact resistance of the tip. At the resonance frequency $f_{res} = 1/(2\pi\sqrt{LC})$, the impedance of the LCR circuit is given by $Z_L = L/CR_{tip}$ without the imaginary part. By adjusting the inductance L and capacitance C, the contact resistance of the tip is transformed close to the impedance of the RF source ($Z_0 = 50\ \Omega$), and the resonance frequency is approximately 150 MHz to provide a wide bandwidth. The change in contact resistance is indirectly detected through the reflectance at the resonance frequency.

Practically, the implementation of a contact resistance-based imaging mechanism requires a cantilever-free elastomeric tip with high electrical conductivity. To meet the material demands, we used a conductive CB-PDMS composite to fabricate the tip. The CB-PDMS composite exploits the percolation network of the conductive CB particles to provide electrical conductivity in the elastomeric PDMS matrix. The density of the percolation network is determined by the fraction of CB embedded in the PDMS matrix. In our case, a high fraction of CB particles is desirable for high conductivity and homogeneity of the composite.[23,24] Considering the processability of the CB-PDMS resin limits the maximum fraction of CB particles, thus we used a CB-PDMS composite with 25 wt. % CB particles to achieve an electrical conductivity of approximately 22 S/m according to previous research.[25]

Figure 2(a) shows the fabrication process of the conductive elastomeric tip using the CB-PDMS composite. A silicon substrate

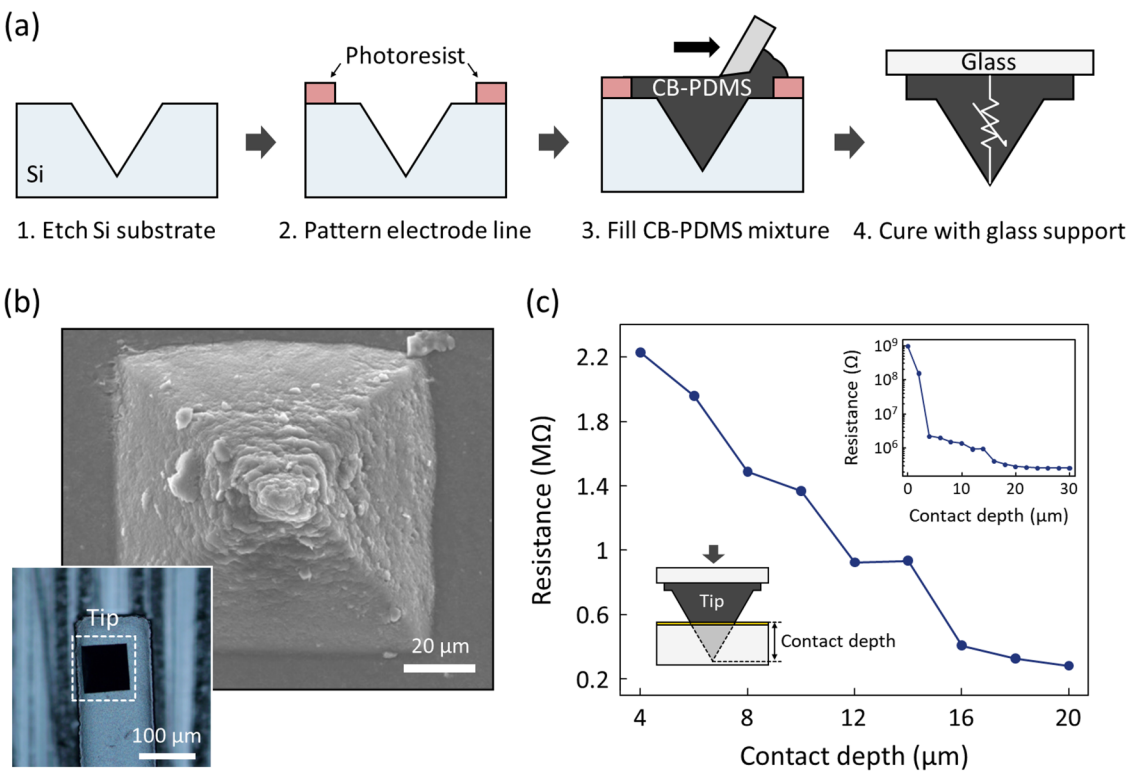

FIG. 2. Carbon black-polydimethylsiloxane (CB-PDMS) tip. (a) Fabrication process of a CB-PDMS tip. (b) Scanning electron microscopy (SEM) images of the CB-PDMS tip. The inset shows the optical microscopy image of the CB-PDMS tip. (c) Resistance depending on the contact depth between the CB-PDMS tip and the conductive surface.

was wet-etched to make a pyramid-shaped mold. The trench to form the electrode line was defined by photolithography using a SU-8 photoresist. The CB-PDMS resin was prepared by vigorous mixing of PDMS (Dow corning, Sylgard 184) and CB particles (Vulcan, XC-72R). The CB-PDMS resin was filled in the etched silicon mold with the SU-8 trench, and then cured at 80 °C for 4 h with the glass support. A scanning electron microscopy (SEM) image in Fig. 2(b) shows the pyramid-shaped CB-PDMS tip. While the surface of the tip was slightly lumpy, the tip apex was approximately 2 μm in diameter. The electrode line connected to the external instrument was well-formed by the CB-PDMS composite [the inset of Fig. 2(b)].

We investigated the contact resistance at the contact depth between the CB-PDMS tip and Au-coated Si wafer [Fig. 2(c)]. In the early stage of contact, the CB-PDMS tip exhibited a high contact resistance of approximately 1 GΩ [the inset of Fig. 2(c)]. This insulator-like behavior of the CB-PDMS tip at a low contact depth, i.e., a small contact area, is attributed to the microscopic inhomogeneity of the percolation path on the surface of the CB-PDMS composite.[24] At a contact depth of 4 μm, the contact resistance decreased to 2.2 MΩ, indicating sufficient conducting sites on the tip apex. Subsequently, the contact resistance decreased linearly as a function of the contact depth [Fig. 2(c)].

To implement RF reflectometry, we constructed the custom-built measurement setup, as described in Fig. 3(a). The measurement setup consisted of a tip, a printed circuit board (PCB), and an external instrument. The tip-PCB contained the LC circuit and the CB-PDMS tip as the resistor [Fig. 3(b)]. External instruments generated RF waves and demodulated the reflected signal. For the RF reflectometry measurement, the RF wave was generated from a function generator and then transferred to the LCR circuit on the tip-PCB. Depending on the impedance of the LCR circuit, different magnitudes of the RF wave were reflected to the demodulator composed of a phase shifter, mixers, and low-pass filters. Two mixers merged the reflected wave with two reference signals with a phase difference of 90°. Finally, a low pass filter cuts the AC components in the mixed signals, generating the outputs, V_{rx} and V_{ry}, which are expressed as follows:

$$V_{rx} = (V_R \sin \phi)/2, \tag{2}$$

$$V_{ry} = (V_R \cos \phi)/2, \tag{3}$$

where V_R and ϕ are the reflectance and phase difference between the reference signal and reflected signal, respectively. From the output voltages V_{rx} and V_{ry}, we calculated the reflectance V_R and phase difference ϕ.

The measurement frequency of the RF wave was determined by the resonance frequency of the LCR circuit. We set the resonance frequency of the LCR circuit to approximately 150 MHz by means of the capacitance and inductance of the LCR circuit. We used two varactors to adjust the LCR circuit *in situ*,[20] which could be needed owing to the deviation of the contact resistance and parasitic capacitance of the CB-PDMS tip. Figure 3(c) shows the typical reflectance of the LCR circuit as a function of the frequency measured by a network analyzer. When the CB-PDMS tip and conductive surface were in contact, the reflectance steeply decreased. Then, the magnitude of the reflectance at the resonance frequency decreased as a function of the contact depth (z).

This reflectance behavior of the LCR circuit was well-reproduced in the custom-built RF reflectometry setup [the inset of Fig. 3(c)]. The sudden change of phase in the RF reflectometry measurement indicates that the resonance frequency of the LCR circuit corresponded to the low reflectance at that frequency. The bandwidth of the LCR circuit was approximately 8.5 MHz as the full width at half maximum, which ideally provides a fast measurement time. However, the practical measurement rate is limited to 5 Hz due to the slow moving speed of the tip and the data acquisition time of the control PC. This wide bandwidth of RF reflectometry is potentially beneficial to detect the signals from massively parallel probe arrays. Figure 3(d) shows the RF reflectometry measurement at the resonance frequency as the response of the vertical movement of the CB-PDMS tip near a contact depth of 5 μm. The reflectance can distinguish 20 nm steps of the vertical movement of the CB-PDMS tip. The precision of the signal was 1.5×10^{-4} as the root mean square of the flat region. This result validates the high-precision electrical detection of the RF reflectometry measurement for cantilever-free imaging.

Finally, we measured the line profiling of the test sample to demonstrate contact resistance-based cantilever-free imaging using RF reflectometry. The test samples were prepared by etching a SiO_2 layer on a Si wafer, followed by thermal evaporation of a 50 nm-thick Au film with a 5 nm-thick Ti adhesion layer. The line profile of the test sample was measured by repeating vertical scanning at a constant scanning distance along the feature. The RF reflectance of each measured point was detected at the end of a vertical scanning distance of 5 μm. Note that the measurement rate of the prototyping SPM system is much slower than the capability of the detection system due to the limited moving speed of the tip and the data acquisition time of the control PC. These steps take 0.1 s to move the tip and 0.1 s to collect and process the signal per each point, and therefore, the practical measurement rate is up to 5 Hz. Although we have demonstrated a simple proof-of-concept, the wide bandwidth of the detection system can be fully utilized with a massively parallel probe array and a developed control system in future works.

Figure 4(a) shows the line profiles of 2 μm-height features measured by RF cantilever-free imaging. The measurement exhibited a clear 2 μm step of the feature, which was well reproduced in three measurements. The precision of the measurement was 210 nm as the root mean square of the flat region. The vertical resolution of our imaging mechanism allows the resolution of sub-micrometer-scale features with a height of 230 nm with a precision of 83 nm as the root mean square of the flat region [Fig. 4(b)]. These results indicate the successful performance of our device in providing high-resolution cantilever-free imaging. We note that the resolution of the line profile was lower than the precision of the vertical movement measurement in Fig. 3(d). For the line profile measurement, the deviation in the individual vertical scanning affects the resolution. We speculate that the conductivity of the CB-PDMS composite itself varied upon each vertical scanning due to the deformation of the tip, which further deteriorated the precision of line profile measurement.

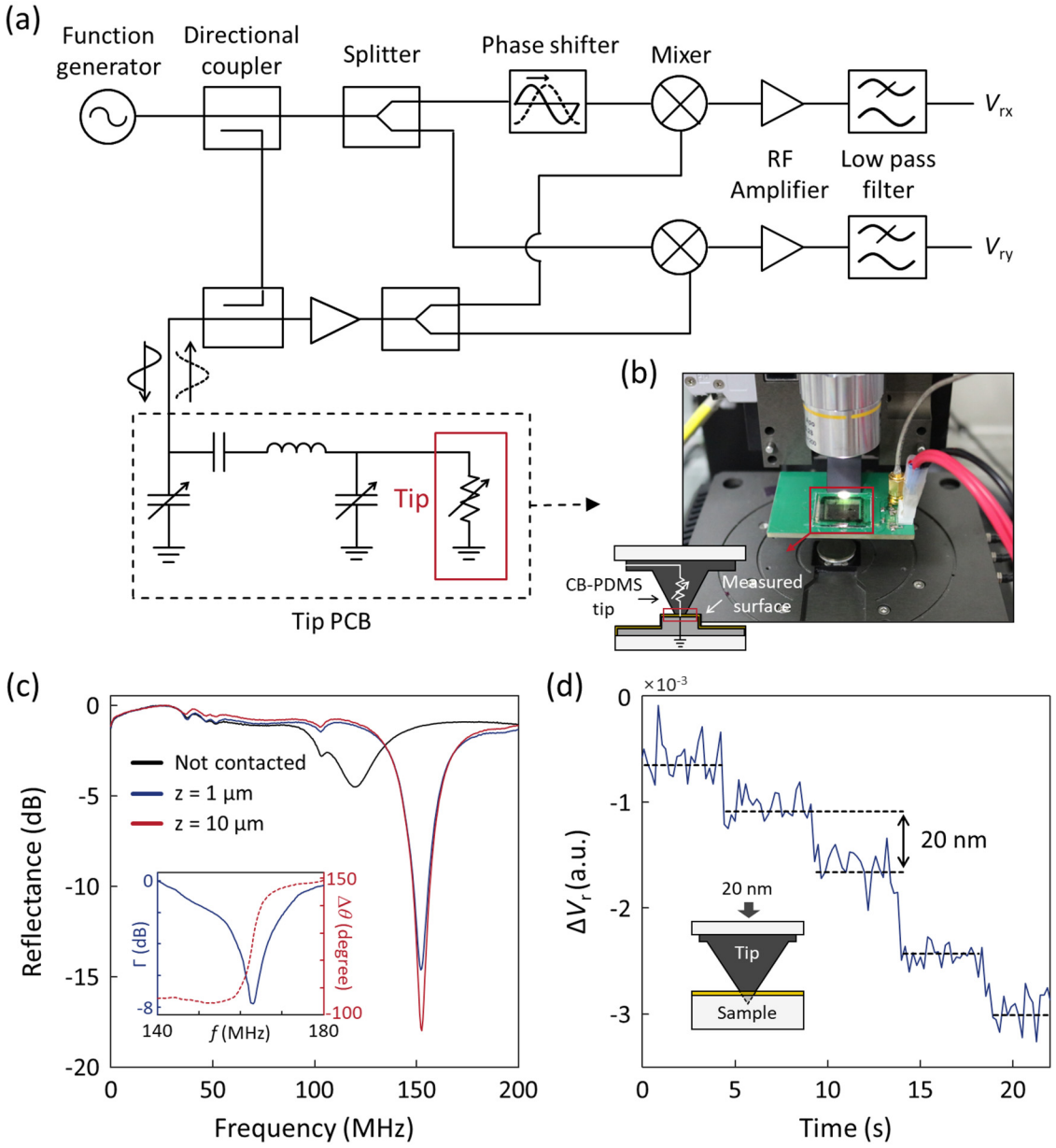

FIG. 3. RF reflectometry measurement setup. (a) Schematic diagram of a RF reflectometry measurement setup. (b) Photograph of a CB-PDMS tip attached to a LCR circuit printed circuit board (PCB). (c) Relative magnitude of reflectance from the LCR resonance circuit as a function of frequency measured by a network analyzer. The inset shows the relative magnitude and phase difference of the reflected signal measured by the RF reflectometry measurement setup depicted in Fig. 3(a). (d) Reflected signal as a response of the vertical movement of the CB-PDMS tip.

RF cantilever-free imaging exhibited high resolving power in the vertical direction, but the line profiles had a gradual slope of features, in contrast to the results of the AFM measurement [the inset of Fig. 4(a) and broken line in Fig. 4(b)]. Similar to other tip-based imaging mechanisms, this artifact originated from the blunt tip apex. Due to the long vertical scanning distance of approximately 5 μm, the contact area of the measurement was approximately $7 \times 7\,\mu m^2$, which would be applicable to the investigation of sheet-like specimens.[26–29] We would like to note that the deformation of the elastomeric CB-PDMS tip itself can reduce the contact force applied to the sample.[15,30] The contact deformation of the sample by a PDMS-based tip is not severe if Young's

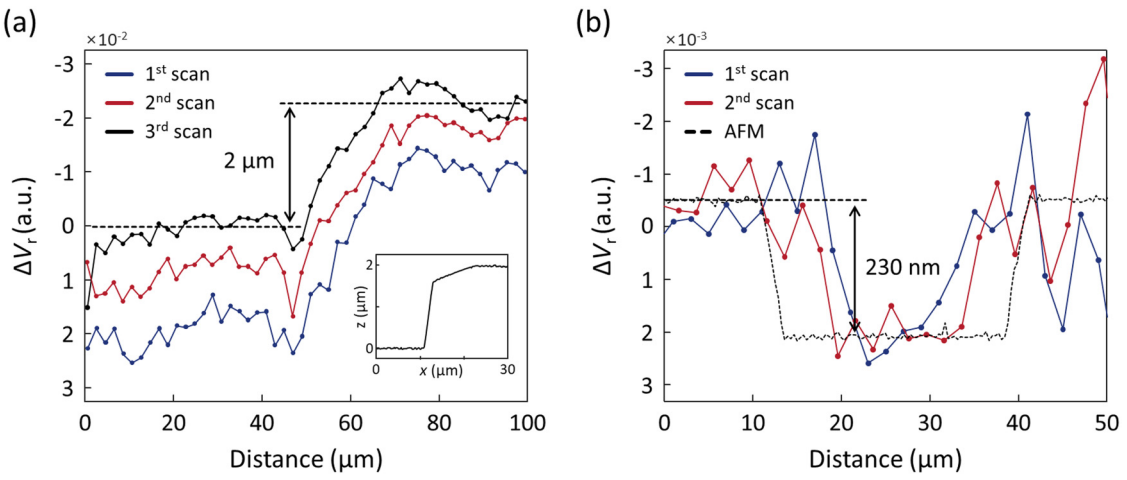

FIG. 4. Line profiling. (a) Line profile of a 2 μm-height feature measured by a RF reflectometry measurement. The inset shows an atomic force microscopy (AFM) measurement of a feature. (b) Line profile of a 230 nm-deep trench.

modulus of the sample is higher than 1 GPa, such as typical hard polymers, ceramics, and metals.[15] Moreover, the contact force would be further reduced by decreasing the crosslinker ratio of PDMS for soft specimens. Regarding the resolution, we expect that the contact area of the tip could be reduced by selecting a tip material with better surface conductance homogeneity, such as conductive polymer[31] and ionic hydrogel[32] in future studies. In addition, increasing the sharpness of the tip through the oxidation sharpening technique of Si mold[33] can further improve the lateral resolution.

III. CONCLUSIONS

We have presented the cantilever-free imaging mechanism adopting the RF reflectometry measurement. The imaging mechanism exploits the change in the contact resistance between the elastomeric conductive tip and conductive surface to measure the height of the feature. The RF reflectometry measurement enabled highly sensitive detection of the contact resistance and achieved nanoscale topography measurements. To demonstrate the feasibility of the imaging mechanism, we fabricated the CB-PDMS tip and constructed the RF reflectometry setup. We obtained a vertical resolution of 230 nm and potential bandwidth of the detection system of approximately 8.5 MHz. Our contact resistance-based imaging system offers advantages over conventional scanning probe microscopy in terms of facile tip fabrication and a simple working mechanism that does not require a feedback system, and therefore, can be easily multiplexed into parallel measurement. Importantly, the high precision and wide bandwidth through RF reflectometry are potentially useful to operate massively parallel cantilever-free SPM, although the proof-of-concept of single-tip imaging was demonstrated at this stage. We would like to note that there are several remaining challenges. First, a conductive elastomer with high spatial homogeneity is needed to achieve nanoscale resolution in the lateral direction as the minimum contact area to make the conducting path determines the lateral resolution. Second, the multiplexing technique of RF reflectometry should be investigated to operate massively parallel probe arrays practically. Further advances in these issues will pave the way for a cantilever-free SPM technique with both high resolution and throughput.

ACKNOWLEDGMENTS

This research was supported by the National Research Foundation of Korea (NRF) grant funded by the Korean government (No. NRF-2018M3D1A1058793).

AUTHOR DECLARATIONS

Conflict of Interest

The authors have no conflicts to disclose.

Author Contributions

Gwangmook Kim: Conceptualization (lead); Data curation (lead); Investigation (lead); Methodology (lead); Software (lead); Visualization (lead); Writing – original draft (lead); Writing – review & editing (lead). **YoungJun Cho:** Data curation (supporting); Investigation (supporting); Methodology (supporting); Writing – original draft (supporting); Writing – review & editing (supporting). **Min-Kyun Cho:** Data curation (supporting); Methodology (supporting). **Dohun Kim:** Conceptualization (lead); Investigation (lead); Methodology (lead); Software (lead). **Wooyoung Shim:** Conceptualization (lead); Funding acquisition (lead); Investigation (lead); Methodology (lead); Project administration (lead); Supervision (lead); Writing – original draft (lead); Writing – review & editing (lead).

DATA AVAILABILITY

The data that support the findings of this study are available from the corresponding author upon request.

REFERENCES

[1]K. S. Novoselov, A. K. Geim, S. V. Morozov, D. Jiang, Y. Zhang, S. V. Dubonos, I. V. Grigorieva, and A. A. Firsov, "Electric field effect in atomically thin carbon films," Science **306**(5696), 666–669, (2004).

[2]G. Binnig, H. Rohrer, Ch. Gerber, and E. Weibel, "7 × 7 reconstruction on Si (111) resolved in real space," Phys. Rev. Lett. **50**(2), 120–123 (1983).

[3]N. Kodera, D. Yamamoto, R. Ishikawa, and T. Ando, "Video imaging of walking myosin V by high-speed atomic force microscopy," Nature **468**(7320), 72–76 (2010).

[4]G. Binnig, H. Rohrer, Ch. Gerber, and E. Weibel, "Tunneling through a controllable vacuum gap," Appl. Phys. Lett. **40**(2), 178–180 (1982).

[5]G. Binnig, C. F. Quate, and Ch. Gerber, "Atomic force microscope," Phys. Rev. Lett. **56**(9), 930–933 (1986).

[6]D. A. Walters, J. P. Cleveland, N. H. Thomson, P. K. Hansma, M. A. Wendman, G. Gurley, and V. Elings, "Short cantilevers for atomic force microscopy," Rev. Sci. Instrum. **67**(10), 3583–3590 (1996).

[7]T. Ando, N. Kodera, E. Takai, D. Maruyama, K. Saito, and A. Toda, "A high-speed atomic force microscope for studying biological macromolecules," Proc. Natl. Acad. Sci. U. S. A. **98**(22), 12468–12472 (2001).

[8]J. D. Adams, B. W. Erickson, J. Grossenbacher, J. Brugger, A. Nievergelt, and G. E. Fantner, "Harnessing the damping properties of materials for high-speed atomic force microscopy," Nat. Nanotechnol. **11**(2), 147–151 (2016).

[9]S. C. Minne, J. D. Adams, G. Yaralioglu, S. R. Manalis, A. Atalar, and C. F. Quate, "Centimeter scale atomic force microscope imaging and lithography," Appl. Phys. Lett. **73**(12), 1742–1744 (1998).

[10]T. Sulchek, R. J. Grow, G. G. Yaralioglu, S. C. Minne, C. F. Quate, S. R. Manalis, A. Kiraz, A. Aydine, and A. Atalar, "Parallel atomic force microscopy with optical interferometric detection," Appl. Phys. Lett. **78**(12), 1787–1789 (2001).

[11]P. Vettiger, G. Cross, M. Despont, U. Drechsler, U. Durig, B. Gotsmann, W. Haberle, M. A. Lantz, H. E. Rothuizen, R. Stutz, and G. K. Binnig, "The 'millipede'—Nanotechnology entering data storage," IEEE Trans. Nanotechnol. **1**(1), 39–55 (2002).

[12]Q. Yang, Q. Ma, K. M. Herum, C. Wang, N. Patel, J. Lee, S. Wang, T. M. Yen, J. Wang, H. Tang, Y.-H. Lo, B. P. Head, F. Azam, S. Xu, G. Cauwenberghs, A. D. McCulloch, S. John, Z. Liu, and R. Lal, "Array atomic force microscopy for real-time multiparametric analysis," Proc. Natl. Acad. Sci. U.S.A. **116**(13), 5872–5877 (2019).

[13]H. Sadeghian, R. Herfst, B. Dekker, J. Winters, T. Bijnagte, and R. Rijnbeek, "High-throughput atomic force microscopes operating in parallel," Rev. Sci. Instrum. **88**(3), 033703 (2017).

[14]W. Cao, N. Alsharif, Z. Huang, A. E. White, Y. Wang, and K. A. Brown, "Massively parallel cantilever-free atomic force microscopy," Nat. Commun. **12**(1), 393 (2021).

[15]G. Kim, E. J. Kim, H. W. Do, M.-K. Cho, S. Kim, S. Kang, D. Kim, J. Cheon, and W. Shim, "Binary-state scanning probe microscopy for parallel imaging," Nat. Commun. **13**(1), 1438 (2022).

[16]F. Huo, Z. Zheng, G. Zheng, L. R. Giam, H. Zhang, and C. A. Mirkin, "Polymer Pen lithography," Science **321**(5896), 1658–1660, (2008).

[17]F. Huo, G. Zheng, X. Liao, L. R. Giam, J. Chai, X. Chen, W. Shim, and C. A. Mirkin, "Beam pen lithography," Nat. Nanotechnol. **5**(9), 637–640 (2010).

[18]W. Shim, A. B. Braunschweig, X. Liao, J. Chai, J. K. Lim, G. Zheng, and C. A. Mirkin, "Hard-tip, soft-spring lithography," Nature **469**(7331), 516–520 (2011).

[19]R. J. Schoelkopf, P. Wahlgren, A. A. Kozhevnikov, P. Delsing, and D. E. Prober, "The radio-frequency single-electron transistor (RF-SET): A fast and ultrasensitive electrometer," Science **280**(5367), 1238–1242, (1998).

[20]N. Ares, F. J. Schupp, A. Mavalankar, G. Rogers, J. Griffiths, G. A. C. Jones, I. Farrer, D. A. Ritchie, C. G. Smith, A. Cottet, G. A. D. Briggs, and E. A. Laird, "Sensitive radio-frequency measurements of a quantum dot by tuning to perfect impedance matching," Phys. Rev. Appl. **5**(3), 034011 (2016).

[21]Y.-Y. Liu, S. G. J. Philips, L. A. Orona, N. Samkharadze, T. McJunkin, E. R. MacQuarrie, M. A. Eriksson, L. M. K. Vandersypen, and A. Yacoby, "Radio-frequency reflectometry in silicon-based quantum dots," Phys. Rev. Appl. **16**(1), 014057 (2021).

[22]U. Kemiktarak, T. Ndukum, K. C. Schwab, and K. L. Ekinci, "Radio-frequency scanning tunnelling microscopy," Nature **450**(7166), 85–88 (2007).

[23]K. Miyasaka, K. Watanabe, E. Jojima, H. Aida, M. Sumita, and K. Ishikawa, "Electrical conductivity of carbon-polymer composites as a function of carbon content," J. Mater. Sci. **17**(6), 1610–1616 (1982).

[24]M. Knite, V. Teteris, B. Polyakov, and D. Erts, "Electric and elastic properties of conductive polymeric nanocomposites on macro- and nanoscales," Mater. Sci. Eng., C **19**(1), 15–19 (2002).

[25]G. Kim, S. Cho, K. Chang, W. S. Kim, H. Kang, S.-P. Ryu, J. Myoung, J. Park, C. Park, and W. Shim, "Spatially pressure-mapped thermochromic interactive sensor," Adv. Mater. **29**(13), 1606120 (2017).

[26]M. M. Tunesi, R. A. Soomro, X. Han, Q. Zhu, Y. Wei, and B. Xu, "Application of MXenes in environmental remediation technologies," Nano Converg. **8**(1), 5 (2021).

[27]A. Iqbal, J. Hong, T. Y. Ko, and C. M. Koo, "Improving oxidation stability of 2D MXenes: Synthesis, storage media, and conditions," Nano Converg. **8**(1), 9 (2021).

[28]A. H.-T. Nguyen, M.-C. Nguyen, S. Cho, A.-D. Nguyen, H. Kim, Y. Seok, J. Yoon, and R. Choi, "Double-gate thin film transistor with suspended-gate applicable to tactile force sensor," Nano Converg. **7**(1), 31 (2020).

[29]Y. Liu, E. Mu, Z. Wu, Z. Che, F. Sun, X. Fu, F. Wang, X. Wang, and Z. Hu, "Ultrathin MEMS thermoelectric generator with Bi2Te3/(Pt, Au) multilayers and Sb2Te3 legs," Nano Converg. **7**(1), 8 (2020).

[30]X. Liao, A. B. Braunschweig, Z. Zheng, and C. A. Mirkin, "Force- and time-dependent feature size and shape control in molecular printing via polymer-pen lithography," Small **6**(10), 1082–1086 (2010).

[31]L. V. Kayser and D. J. Lipomi, "Stretchable conductive polymers and composites based on PEDOT and PEDOT:PSS," Adv. Mater. **31**(10), 1806133 (2019).

[32]C. Yang and Z. Suo, "Hydrogel ionotronics," Nat. Rev. Mater. **3**(6), 125–142 (2018).

[33]H. Im and S.-H. Oh, "Oxidation sharpening, template stripping, and passivation of ultra-sharp metallic pyramids and wedges," Small **10**(4), 680–684 (2014).